Journal of Non-Crystalline Solids 515 (2019) 75–81

Contents lists available at ScienceDirect

Journal of Non-Crystalline Solids

journal homepage: www.elsevier.com/locate/jnoncrysol

Evidence of the coexistence of multivalence cerium oxide nano-particles in a sodium borate glass

Kisa S. Ranasinghe[a,*], Rajnish Singh[b], Delbert E. Day[c], Klaus Attenkofer[d], Eli Stavitski[d], Lon A. Quinn[a], Diane Patterson[a], Andrew Duenas[b]

[a] Department of Physics, Kennesaw State University, Marietta, GA 30060, United States of America
[b] Department of Chemistry and Biochemistry, Kennesaw State University, Kennesaw, GA 30060, United States of America
[c] Department of Ceramic Engineering, Graduate Center for Material Research, Missouri University of Science and Technology, Rolla, MO 65409, United States of America
[d] Brookhaven National Laboratory NSLSII, Upton, NY 11973, United States of America

ARTICLE INFO

Keywords:
Glass
Nanoparticles
Cerium oxide
Multivalences

ABSTRACT

A sodium borate glass containing both trivalent cerium oxide and tetravalent cerium oxide states nano particles of 2–5 nm in size was successfully prepared by doping the glass with varying amounts of cerium (IV) oxide with. X-ray absorption spectroscopy measurement was used to determine the coexistence of the multivalent state of cerium oxide in the borate glass. Significant changes in the trivalent and tetravalent cerium oxide concentrations were observed when the glass was melted using different melting parameters and different raw materials. Glass made with borax that contained of 0.05mols of CeO_2 and melted at 1100 °C for 3 h had the highest concentration of trivalent cerium oxide. Transmission electron micrographs confirmed the release of trivalent Ce_2O_3 and tetravalent CeO_2 nanoparticles from the glassy matrix. Fourier transform Infrared measurements suggest that the CeO_2 in the glass acts as both a glass-former and glass modifier.

1. Introduction

Cerium oxide (CeO_2) has been of interest in recent years due to its many applications such as a catalyst, and in scintillators, fuel cells, oxygen sensors [1,2], and biomaterials [3]. Unlike the other lanthanide elements, Ce can exist in both trivalent Ce3+ (Ce2O3 -reduced) and tetravalent Ce4+ (CeO_2-oxidized) states as it has two partially filled subs-shells, 4f and 5d, allowing several excited states [4–6]. Cerium oxide is usually in the form of Ce4+ with stable electronic configuration where every oxygen surrounded by a cerium is in a tetrahedral position. Trivalent Ce3+ originates from the transition of *5d* levels to the *2f* ground state, but Ce3+ has the potential to form Ce^{4+} by losing a *4f* electron to by direct ionization or by trapping a hole [7]

$$Ce^{3+} + h^{+} \rightarrow Ce^{4+}$$

$$Ce^{4+} + e^{-} \rightarrow Ce^{3+}$$

In order to understand this multivalence existence an Arrhenius-based equation is modeled [8] for the high temperature reduction and oxidation of CeO_2. Since this reaction

$CeO_2 CeO_{2-\delta} + \frac{\delta}{2}O_2$is an equilibrium reaction, both reduction or oxidation reactions can take place at any given time. This ability to form mixed valence state ceria nanoparticles is useful in many biological and industrial applications [9–17]. When cerium oxide is present in a borate glass a significant amount of cerium oxide is present as the less stable Ce3 + configuration with an oxygen vacancy due to $5d \rightarrow 4f$ emission [9–11]. When CeO_2 is added to the glass, trapped electron centers and trapped hole centers are inhibited and the multi-valent Ce3+ and Ce4+ ions coexist within the glass network. This gives rise to new properties and a new bioglass due to the multivalent ceria nanoparticles [16–18].

Cerium oxide nanoparticles have also been found to have antioxidant properties [17,18] and are able to scavenge and neutralize toxic radicals generated in living systems by oxygen consuming processes as well as environmental conditions [12,19]. The accumulation of these toxic radicals have been implicated in a host of diseases such as cancer, diabetes, Alzheimer's and inflammatory conditions [13,19].

Currently, the formation of polyvalent nanoceria, within a glass, with a specific ratio of Ce^{3+}/Ce^{4+} is not well understood. Moreover, no studies have addressed what ratio is required for cell survival and antioxidant properties, but there is an understanding that the cerium oxide ratios affect the antioxidant activity [19].

in the present study, a glass that is stable against crystallization and is soluble in distilled water was synthesized by doping with CeO_2 to

* Corresponding author at: Department of Physics, Kennesaw State University, Marietta Campus, Marietta, GA 30060, United States of America.
E-mail address: kranasin@kennesaw.edu (K.S. Ranasinghe).

https://doi.org/10.1016/j.jnoncrysol.2019.04.001
Received 11 December 2018; Received in revised form 7 April 2019; Accepted 8 April 2019

produce both trivalent Ce3+ (Ce_2O_3) and tetravalent Ce4+ (CeO_2) nanoparticles. These mixed-valence-state nanoparticles are hermetically sealed within the glass when heat treating the glass during cooling [20]. These nano particles are released from the glass when dissolved in water.

In order to study the cerium valence states in the novel glass, in-situ valence states of Ce3+ and Ce4+ was determined using X-ray Absorption Near Edge Structure (XANES) spectroscopy. XANES data was obtained at Ce L3 edge for all the glass samples at the Inner Shell Spectroscopy (ISS) beamline at the National Synchrotron Light Source II at the Brookhaven National Laboratory. XANES spectroscopy can measure in-situ valence states of redox-sensitive elements such as cerium with a much higher accuracy when compared to X-ray photoelectron spectroscopy which can reduce additional Ce4+ to Ce3+ under high-vacuum, thus overestimating the Ce 3+ concentration. XANES can circumvent this limitation and, therefore, is a more appropriate technique to study the in-situ valence states of Ce3+ and Ce4+ [21-24] Synchrotron based determinations of the amounts of Ce3+/Ce4+ in materials have traditionally used Ce L3-edge XANES which involves a 2p → 5d transition located around 5.7 keV [221-23]. This method was also used to determine the amounts of Ce3+ and Ce4+ in the borate glass containing different amounts of cerium oxide. Further, the glass was physiochemically characterized by Fourier Transform InfraRed (FTIR) spectroscopy and Differential Thermal Analysis (DTA) and the released nanoparticles were investigated via Transmission Electron Microscopy (TEM)

2. Experimental method

2.1. Glass fabrication

A sodium borate glass with molar composition of $Na_2O{\cdot}2B_2O_3$ was used as a parent glass (S1 Glass in Table 1) to create a series of borate glass doped with varying concentrations from 0.01 to 0.05 mol% of CeO_2. Each glass was melted in a platinum crucible in an air atmosphere. The raw materials, boron trioxide and sodium carbonate were obtained from Alfa Aesar with 99.99 purity and another group of glasses S6-1 to S6-5 in 0.05 mol% of cerium (IV) oxide were melted at 1100 °C, 1200 °C and 1300 °C for 1, 2, and 3 h contained borax (sodium tetraborate decahydrate) in raw materials (Table 2). Additionally, for the borate glass that contain 0.05 mol% of CeO_2, raw materials were introduced in the form of sodium tetraborate (S-13), and boric acid (S-14) that produces the same parent glass, to obtained different oxygen reduction levels as indicated in Table 1. Glass S-12 was melted with CeF_3, rich in Ce^{3+} instead of CeO_2 along with boron trioxide and sodium carbonate Each glass was melted in at temperatures and times specified in Table 3. Each melt was given a quick stir in every 30 min and was poured and quenched between two steel plates. The quenched glass was then ground in to powder where the particle sizes ranged from 50 μm to 450 μm. Each poured glass was investigated via optical microscope to observe possible undissolved CeO_2 particles in the glass.

Table 1
Composition/Identification for glasses Na2O·2 B2O3·$xCeO_2$ melted at 1100 °C, for 1 h and melted in the air atmosphere.

Glass ID	Amount of (x) CeO_2 mols
Glass S1	0
Glass S 2	0.01
Glass S 3	0.02
Glass S 4	0.03
Glass S 5	0.04
Glass S 6	0.05

Table 2
Glass Composition/Identification with change in melting temperature and meting time for glass melted in the air atmosphere that contained borax.

Glass ID	Melting Temperature (°C)	Melting Time (hrs.)
Glass S 6-1	1100	1
Glass S 6-2	1100	2
Glass S 6-3	1100	3
Glass S 6-4	1200	1
Glass S 6-5	1300	1

Table 3
Glass Composition/Identification with change in raw materials, melted at 1100 °C, for 1 h. in the air atmosphere.

Glass ID	Raw Materials
Glass S6-1	0.05 mol CeO_2 with Borax
Glass S13	0.05 mol CeO_2 with Tetraborate
Glass S14	0.05 mol CeO_2 with Boric Acid
Glass S12	0.05 mol CeF_3 with Borax

2.2. Extracting nano particles and observing via TEM

A 625 mg of glass powder with a particle size 150 μm was dissolved in 25 ml distilled water (DI) overnight at 37 °C. The solution was then centrifuge and the nanoparticle suspension was separated and sonicated for 5 min with fresh DI water. Then the solution was centrifuged and the process was repeated several times to completely remove the glassy substrate [20]. The final sonicated solutions that included the cleaned nano particles were used to examine the microstructure using Transmission electron Microscope (FEI Tecnai 30 TEM). A small drop of the nano particle solution is then placed on the TEM copper grid followed by overnight drying. The sizes of the nanoparticles as well as the inter atomic distances of these ceria nano particles was observed and measured. .

2.3. Thermal analysis

A DSC Q600 differential Thermal analyzer was used to measure the glass transition temperature (T_g), crystallization peaks (T_c), and melting point (T_m) of each glass A 30 mg sample of glass powder (400–450 μm) was measured and tested by heating the sample to 900 °C at 20 °C/min. The entire set of borate glass was tested, and the thermographs were obtained for comparing the T_g, T_c, and T_m with the parent S1 glass and to measure the Hurby parameter of glass stability against crystallization.

2.4. XANES spectroscopy

XANES measurements were performed at Ce L_3 edge XAS, at NSLS-II, using the 8-ID ISS beamline with an energy range of 4.9 keV–36 keV. The glasses were prepared by a pellet press to create a smooth flat dense sample of 2-3 mm thickness. The data was collected and analyzed using Athena software to calculate Ce+3 and Ce+4 concentrations.

2.5. FTIR absorption spectroscopy

To determine the effects of Cerium Oxide on glass structure, FTIR absorption spectra were recorded at room temperature for all the samples between 600 and 4000 cm^{-1}using a Perkin Elmer ATR-IR Spectrum Two Spectrometer. The instrument was manipulated, and the data was collected using “Spectrum 10” software.

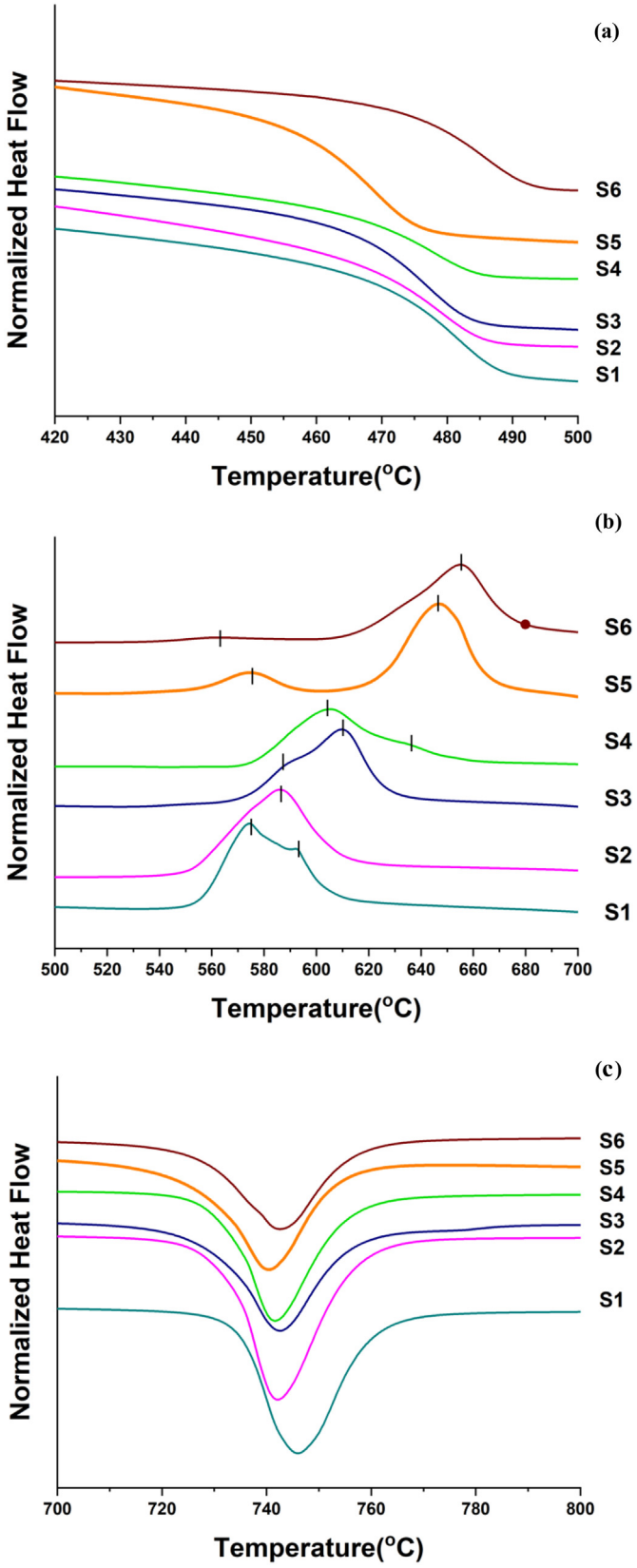

Fig. 1. DSC thermographs of (a) glass transition (b) crystallization and (c) melting temperature for S1 to S 6 glass with increasing CeO_2 content.

3. Results

3.1. Thermal analysis

Each glass was analyzed using Differential Scanning Calorimetry (DSC) to observe any changes in glass transition, (T_g), crystallization (T_c), and melting point (T_m), as the doping concentration of cerium (IV) oxide changes. All thermographs showed a similar glass transition temperature region while some glass samples showed a dual exothermic crystal peak for some concentrations. The DSC thermographs for all the cerium concentrations are shown in Fig. 1, where thermograms have been normalized with respect to 1 mg of mass for all the glasses for better comparison. The glass transition temperature, T_g falls within the same temperature range for all the glasses except S5. The crystallization temperature (T_c) changes as the cerium content in the glass increases. All the glasses have a higher crystallization temperature T_c than the parent (S1) glass without cerium. There are two crystallization peak temperatures; T_{Pk} for S1 glass at 575 °C and 592 °C. The second T_{Pk} of the parent glass was significantly smaller and the dominant peak temperature increases with increasing cerium content. All glass samples have dual crystallization peaks and the peak temperatures are labeled in Table 4 with the exception the S2 glass which was melted with 0.01mols of CeO_2. The melting temperature T_m is similar in all the glass compositions.

3.2. TEM microstructure analysis

Coexistence of the mixed-valence-state Ce^{3+} (Ce_2O_3) and Ce^{4+} (CeO_2) nanoparticles were observed. Glass S6 was dissolving in DI water at 37 °C for different times to determine the presence of ceria nanoparticles and TEM images for 2 h of dissolution are shown in Fig. 2, with (a) shows a fairly low magnification image with agglomerated ceria nano particles with agglomerated ceria nano particles while figure (b) shows a higher resolution image overlapping ceria nano particles and (c) with higher resolution image showing ceria nanoparticles ranging from 2 to 5 nm. Fig. 3 displays two enhanced images of nanoparticles after glass S6 was dissolved in DI water for (a) 7 h and (b) 2 h. Both micrographs show evidence of nano particles with atomic distances of (0.388 ± 0.002) nm, (0.245 ± 0.002) nm, and (0.422 ± 0.002) nm confirming the presence Ce_2O_3 nano crystals and the measured inter atomic distances of (0.311 ± 0.002) nm and (0.386 ± 0.002) nm are in complete agreement to the lattice parameter of CeO_2 [25-33]. Results demonstrate that the ceria nanoparticle size didn't change considerably with hours of dissolution while the particles recovered after dissolved in DI water are in sizes ranged from (2.02 ± 0.005)nm to (4.75 ± 0.05)nm as shown in the high-resolution image in Figs. 2(c) and 3(c).

3.3. XANES spectral analysis

Glasses were studied with XANES at Ce L $_3$ edge and compared to reference compounds CeF_3 and CeO_2. The XANES spectrum of the trivalent cerium (CeF_3-Ce^{3+}) is dominated by the single peak at 5727 eV

Table 4
Glass transition, (T_g), Crystallization on-set (T_c), Crystallization Peaks (T_{Pk1}) and (T_{Pk2}) and melting (T_m) temperatures (± 0.5 °C), as the concentration of CeO_2 increases in the glass along with the calculated Hruby parameter, K_H [39].

Glass ID	T_G(°C)	T_C(°C)	T_{Pk1}(°C)	T_{Pk2}(°C)	T_m(°C)	K_H
S1	471	553	575	592	724	0.48 ± 0.003
S2	469	364	586	–	711	0.65 ± 0.004
S3	467	570	589	610	710	0.74 ± 0.004
S4	468	572	605	637	718	0.71 ± 0.004
S5	459	553	575	645	670	0.80 ± 0.006
S6	474	607	562	655	712	1.27 ± 0.008

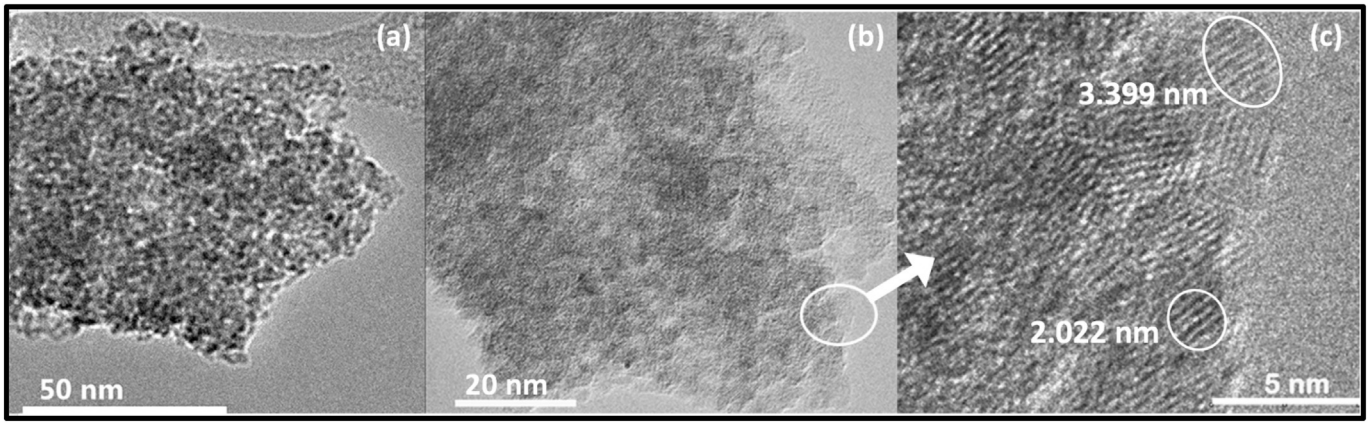

Fig. 2. (a) Low resolutions (b) Higher resolution TEM image of cerium oxide nanoparticles from S6 glass that was dissolved in DI water at 37 °C. (c) size of the cerium oxide nanoparticles that was created within the S6 glass that was dispersed in DI.

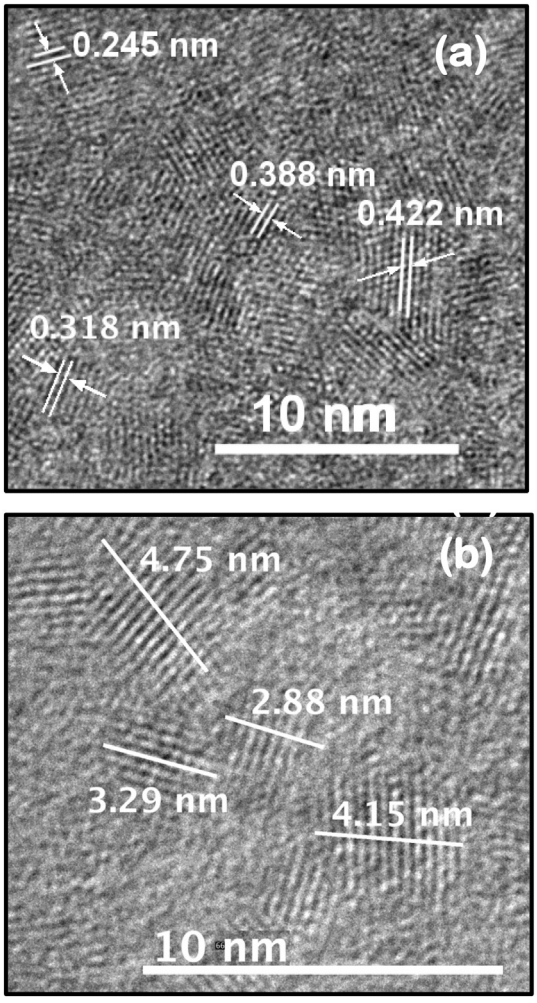

Fig. 3. (a)Atomic distance of CeO_2 nanoparticles recovered from S6 glass after it was dissolved in DI water. (b) size of CeO_2 nanoparticles from S6 glass after dissolved in DI water.

whereas tetravalent reference (CeO_2-Ce^{4+}) shows a double peak at 5731 eV and 5738 eV as shown in Fig. 4. Fig. 5 shows the XANES spectrum as the amount of CeO_2 in the glass increases for glasses melted at 1100 °C for 1 h. Glass S2 shows a higher Ce^{3+} contribution while Ce^{4+} is more pronounced in glass S5. The temperature and time affect the redox states were observed and measured using the XANES spectra

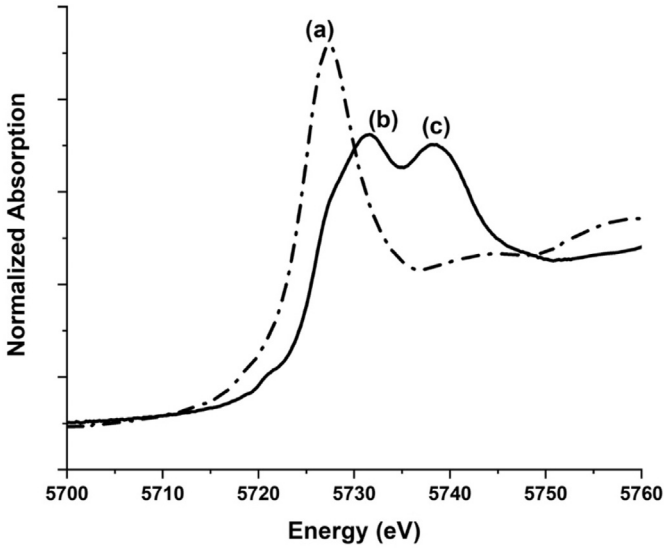

Fig. 4. Ce L_3 edge XANES spectrum for the reference crystalline compounds $CeF_3(Ce^{3+})$ (.-.) and $CeO_2(Ce^{4+})$ (−) with (a) trivalent (Ce^{3+}) due to $5d \rightarrow 4f$ emission, and tetravalent reference (Ce^{4+}) due to $2p \rightarrow 5d$ with final state (b) *2p4f15d1* (c) with *2p5d*.

as shown in Fig. 6 (a) for glass with 0.05 mol% of CeO_2 with borax used in the raw material. The Ce^{3+} peak height increased with increasing melting time for glasses melted at 1100 °C. When the glass was melted at remaining temperatures for 1 h, the glasses melted at 1000 °C and 1300 °C had similar Ce^{3+} peak heights. The glass melted at 1100 °C for 3 h had the highest Ce^{3+} peak height out of all the melts. In order to further understand the different mechanisms of oxygen reduction of the glass, the glass with 0.05 mol% of CeO_2 was melted using different raw materials, such as borax, tetraborate, boric acid, and cerium fluoride. Fig. 6 (b) shows the XANES spectra for the glass melted with different raw materials to obtain 0.05 mol% Ce. According to these results, the glass doped with CeF_3 had the higher Ce $^{3+}$ concentration compared to the glass melted with CeO_2.

3.4. FTIR spectral analysis

The FTIR spectra of the S1 parent glass along with the glasses of varying CeO_2 content are shown in Fig. 7(a). Significant changes in the peaks were observed as the cerium content of the glass increased. IR spectra of the parent S1 glass shows a peak between 600 cm^{-1} to 850 cm^{-1} due to bending vibrations of various borate segments while the bending vibrations of the B-O-B linkage is shown by the small peak

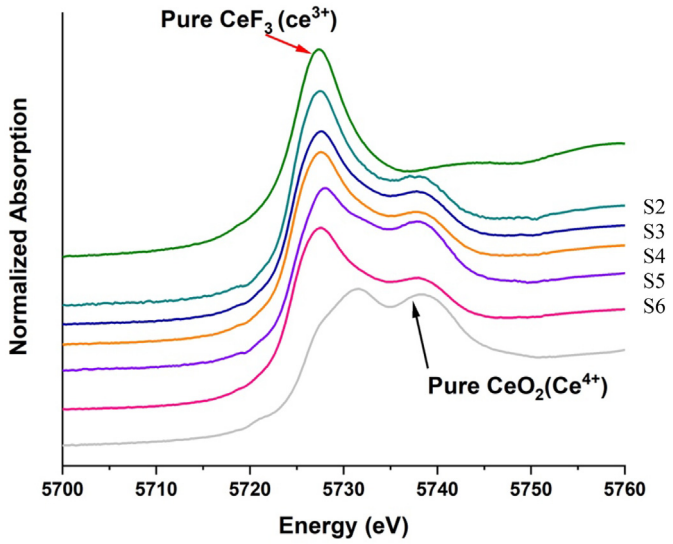

Fig. 5. XANES spectrum for the glasses containing from 0.01 to 0.05 mols of CeO_2 compared to the spectrum for pure CeF_3 (Ce^{3+}) and pure CeO_2(Ce^{4+}).

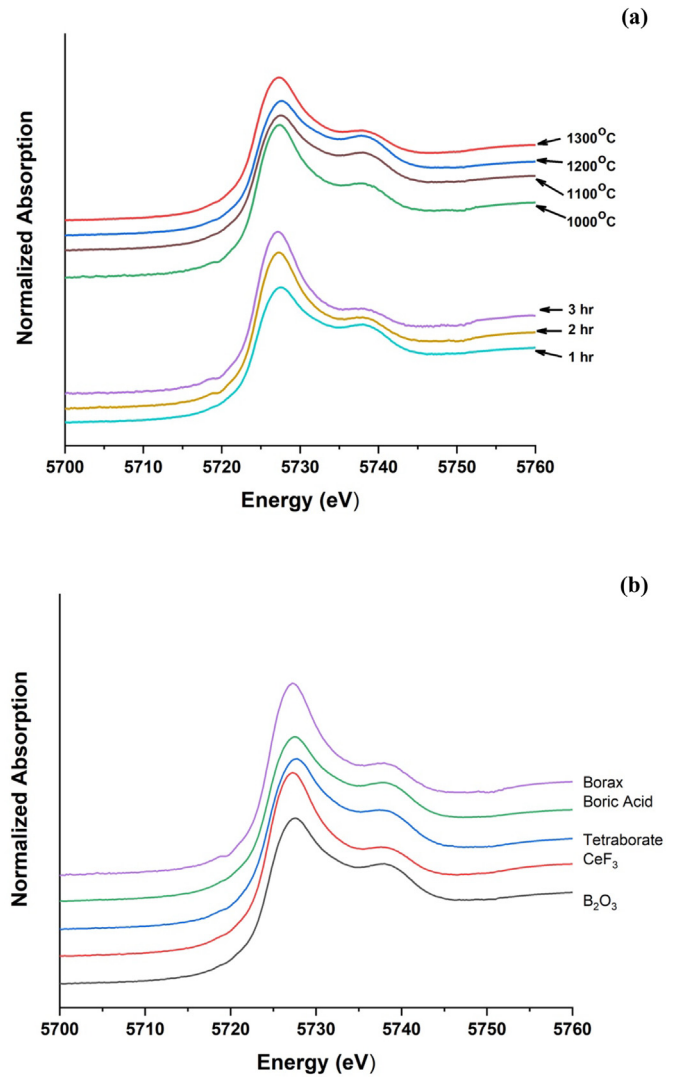

Fig. 6. XANES spectra for S6 glass with 0.05mols of (a) cerium with different melting temperature and melting time (b) melted with different raw materials.

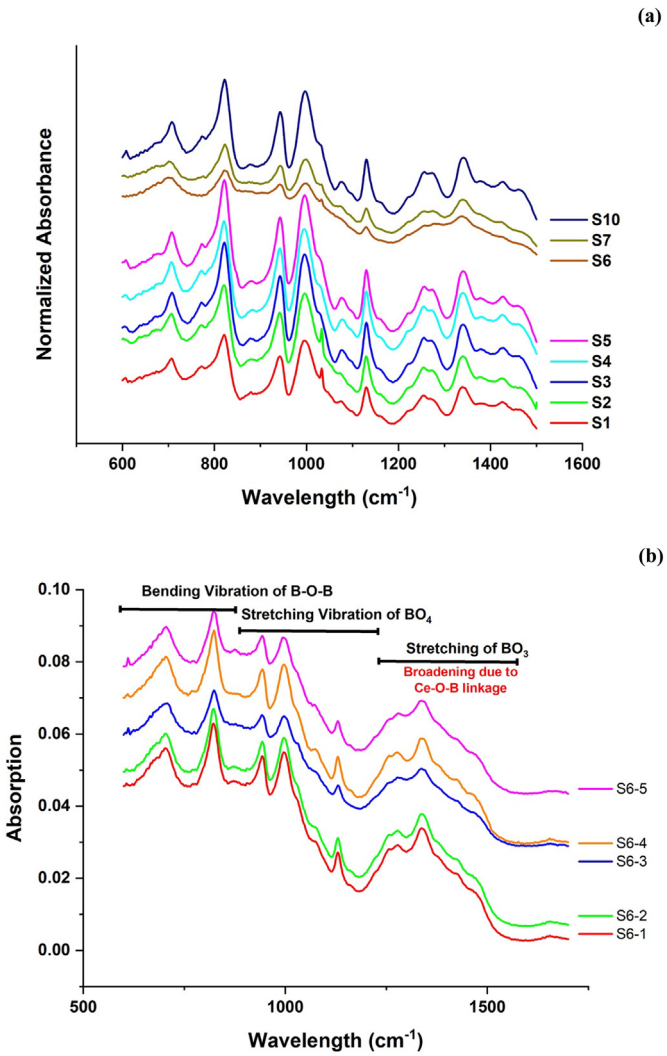

Fig. 7. FTIR spectra (a) S1 with increased cerium content (b) S6 glass with different melting time and temperature.

at 710 cm^{-1} [33,34]. The spectral lines between 850 cm^{-1} to 1200 cm^{-1} attribute to B—O stretching vibrations of BO_4, while region between 1200 cm^{-1} and 1500 cm^{-1} is associated with B—O stretching vibrations of BO_3 units [33-35]. Peaks around 775, 880, 1034, 1220, 1345 and 1432 cm^{-1} seem to decrease in height as the cerium content in the glass increased and completely disappear in the S6 glass. The peak begins to reappear and increase in height with increasing the cerium in the glass. Peaks at 823, 936, 997, 1133, and 1226 cm^{-1} increased in height with increasing cerium content but rapidly decreased in height with 0.05 and 0.06 mols of CeO_2 and again increased in height with further increase in Ceria. These results indicate that glasses S5 and S6 containing 0.05 and 0.06 mols of CeO_2 respectively are notably different from the rest of the glasses containing cerium and that of the parent glass.

4. Discussion

The glass containing Na2O and B2O3 was mixed in with several different amounts CeO_2 to study the development of multivalent CeO_2 and Ce_2O_3 nano particles created within the glass due to different oxygen reduction conditions. The first set of data was obtained from changing the number of CeO_2 mols in small quantities, as 0–0.05 mols of CeO_2. The second set was obtained by changing the melting time and temperature while keeping doped amount of CeO_2 constant; 0.02 and

0.05 mols. The third set was obtained by introducing different raw materials to achieve different reduction status. The DSC micrographs shows that the melting temperature of these glasses are around 700 °C and the glass was melted at 400–600 °C above the melting point to achieve the full dissolution of CeO_2 and CeF_3 and a higher homogeneity. The optical micrographs conducted for all the glasses shows no evidence of undissolved CeO_2 particles. The DSC micrographs shows that the glass transition region is similar in all compositions even though T_g changes with the added CeO_2 amount. These samples had pronounced but different crystallization temperatures with a similar trend like T_g exhibiting an increase with added CeO_2 amount. The Glass-forming ability, which relates to the ease by which melts can be cooled to form glasses with the avoidance of crystal formation [36], remains similar to the parent glass as CeO_2 content increases since the glass transformation region and the glass melting temperature regions remains similar to each another. On the other hand, the glass stability, which was calculated using Hruby parameter, KH [37], differ as the amount of CeO_2 content increases as shown in Table 2. Glasses with higher K_H are stable against crystallization upon reheating, indicating changes in the glass network as the cerium content changes, which is confirmed by FTIR Spectroscopy. Glass composition with 0.05mols of CeO_2 (S6, S13 and S14) have the highest stability against crystallization.

Strong evidence of the coexistence of multivalence CeO_2 and Ce_2O_3 nanoparticles was observed when the nanoparticles were recovered from these glasses by dissolving the powdered glass in DI water. As discussed earlier, the CeO_2 easily interchange to more reduced Ce_2O_3 by exchanging oxygen, creating a hexagonal structure from a more fluoride structure. High resolution FEI Tecnai 30 TEM measurements are in a very good agreement with the known atomic distances of CeO_2 and Ce_2O_3 structures. As shown in Fig. 3, the measured inter atomic distances of (0.311 ± 0.02) nm are in complete agreement to the ideal lattice parameters of the cubic structure of CeO_2 [25-27]. Additionally, inter atomic distances of (0.388 ± 0.02) nm and (0.386 ± 0.02) nm are in complete agreement to the lattice parameter of A-type hexagonal structure of Ce_2O_3 (0001) plane interatomic distance of 0.3888 nm [28]. The atomic distances (0.242 ± 0.03) and (0.422 ± 0.03) nm refers to (200) of and (101) planes of the hexagonal Ce_2O_3 nano particles [25,27-30]. Both TEM micrographs shown in Fig. 2(c) and 3(c) provide evidence of the coexistence of both types of cubic structure of CeO_2 and hexagonal Ce_2O_3 nano particle in the range of 2 to 5 nm in size. The shapes and the sizes of these particles are in very good agreement with the nano particles obtained by Day et al. [20].

The results obtained from the XANES measurements using Ce L_3 edge confirms the coexistence of the two valences Ce^{3+} and Ce^{4+} in the glass when doped with CeO_2 (Ce^{4+}). All the glasses measured via XANES were compared to compounds CeF_3 (Ce^{3+})and CeO_2. Results shows trivalent (Ce^{3+}) with a strong narrow single peak as shown in Fig. 3 (a) due to $5d \rightarrow 4f$ emission while the tetravalent reference (Ce^{4+}) shows a multi-peak. Peak (c) in Fig. 3, due to the transition where electron is exited from Ce 2p to 5d with no electron in the Ce 4f shell, while peak Fig. 3 (b) which is also a Ce^{4+} peak where final state is 2p4f15d1. In addition to an electron exited from the valence 2p to 5d, another electron is excited from the valence band of Oxygen 2p shell to Cerium 4f shell leaving a hole [24]. None of the glass compositions exhibited this forbidden peak (b) which denotes that an electron is excited only from the Ce 2p shell to its 5d shell. These results were comparable to the results of Cicconi et al. [7] thus providing strong evidence of the coexistence of the both trivalent (Ce^{3+}) and tetravalent (Ce^{4+}) with in the glass. Out of all the glasses melted with B_2O_3, S2 glass melted with 0.01 mols of CeO_2 for 1100 °C for 1 h had the highest amount of Ce^{4+}.

ions, while glass S6–2 melted with borax and 0.05 mols of CeO_2 for 1100 °C for 3 h had the highest amount of Ce^{3+} ions out of all meted glass samples, reaching higher oxidization to reduced status. When the same composition of S 6 glass with 0.05 mol of CeO_2 is melted at different melting times, the Ce^{3+} concentration increases as the melting time increases as shown in Fig. 6(a). Glass melted at 1200 °C had the highest Ce^{4+} concentration. The Ce^{3+} concentration of S12 glass melted with CeF_3 (rich in Ce^{3+}) is similar to S2 glass melted with different melting times using 0.01 mol of CeO_2. Significant changes in the Ce^{3+} peak height was not observed when the same S6 glass composition was made with borax (S6–1), tetra borate (S13) and boric acid (S14) instead of using raw materials of B_2O_3 and Na_2CO_3 and melted for 1100 °C for 1 h. Out of all the glasses made with borax, the S6–3 glass made with borax for 3 h had the highest amount of Ce^{3+} concentration.

Each of the glass samples except the glasses labeled S12-S14 were processed using B_2O_3 as part of the composition. Vitreous B_2O_3 consist of BO_3 unit associated to form Boroxol rings which produces a spectral band at 806 cm^{-1} in the glassy matrix [38]. The Na_2O present in the glass convert BO_3 units to BO_4 units [34,35]. The peak at 1034 cm^{-1} in the parent glass S1 is due to the bond stretching vibrations of BO_4 while 775 cm^{-1} peak is comparable to the bind bending vibrations of BO_4. Spectral lines at 1345 and 1432 cm^{-1} in the FTIR absorption spectra are comparable to B—O stretching of trigonal BO_3 units [35]. The lack of a peak at 806 cm^{-1} in the absorption spectra in any of the glass tested indicate that the glass network mainly consists of BO_3 units to BO_4 units at the expense of boroxol rings. However, adding CeO_2 to the glass network works much differently than adding alkali as discussed in Damwari et al. CeO_2 act as a glass modifier as well as a glass network former [33]. Both BO_3 units to BO_4 units in the IR spectra of the S6 glass disappeared indicating a formation where BO_3 units would be used to form Ce-O-B units rather than BO_4 units. It has been investigated that [33] the asymmetric stretching vibrations of Ce-O-B lies in the 400 and 1370 cm^{-1}. All the glasses formed from 0.05 mol of cerium oxide, S6-1 to S6-5 show the same significant difference that the S6 glass shown in the IR spectra with a peak broadening from 1200 to 1600 cm^{-1} as shown in Fig. 7(b). This could be due to the existence of both active bands of Ce-O-B and B-O-B links overlapping in this series of glass. The formation of Ce-O-B link as a glass former is supported by the XANES data where glass with 0.05 mol (specially S6-2) showed the highest amount of oxygen reduction providing larger amount of non-bridging oxygen (NBO) in the glass, forming much stable Ce-O-B link.

5. Conclusion

A soluble sodium borate glass containing varying amounts of cerium oxide that is stable against crystallizations was successfully prepared with both trivalent Ce3+ (Ce2O3) and tetravalent Ce4+ (CeO_2) states. Cerium oxide nano particles were released when these glasses were dissolved in DI water. The TEM data provides strong evidence of coexistence of both types of cubic structure of CeO_2 (tetravalent Ce4+) and hexagonal Ce_2O_3 (trivalent Ce3+) nano particles. The concentrations of Ce3+ and Ce4+ in these glasses were determined using XANES Ce L3 edge x-ray absorption spectroscopy. The XANES results also confirmed the coexistence of Ce3+ and Ce4+ valences in a series glasses with different concentrations of CeO_2 (Ce4+) melted with different temperatures, times, and raw materials. The Ce3+ and Ce4+ amounts significantly differed as the amounts of CeO_2 changed as well as with changes in melting time, temperature and raw materials. Glass S6–2 with 0.05 mol% CeO_2 had the maximum amount of Ce2O3 (Ce3+) while glass S5 with 0.04 mol% CeO_2 had the maximum amount of CeO_2 (Ce4+). The results of this work also confirmed that the cerium oxide in the glass acts as both network modifier and network former. Cerium in the glass contained higher order Ce3+ act as a glass network former by creating a Ce-O-B link instead of BO_4 units while the glass with higher concentration of Ce4+ use cerium as a network modifier by creating BO_4 units from BO_3 units with increasing addition of CeO_2.

Acknowledgment

This work is supported by the funds from Kennesaw State

University. This research used beamline 8-ID (ISS) of the National Synchrotron Light Source II, a U.S. Department of Energy (DOE) Office of Science User Facility operated for the DOE Office of Science by Brookhaven National Laboratory under Contract No. DE-SC0012704. Further the authors acknowledge Mohammed Odeh, Peyton Butler, Ki Dae Kim, Tatum Nicewander, and Duncan Bohannon for their assistance in various aspects of this study.

Declaration of interests

The authors declare that they have no known competing financial interests or personal relationships that could have appeared to influence the work reported in this paper.

The authors declare the following financial interests/personal relationships which may be considered as potential competing interests: none.

References

[1] Xiaowu He, Xiaofang Liu, Rongfeng Li, Bai Yang, Yu Kaili, Min Zeng, Yu Ronghai, Effects of local structure of Ce^{3+} ions on luminescent properties of $Y_3Al_5O_{12}$:Ce nanoparticles, Nat. Sci. Rep. 6 (2016) 22238.

[2] M. Bosca1, V. Pop, E. Culea, I. Vida-Simiti, Spectroscopic Properties of Cerium-Boro-Bismuthate Glasses, Studia Ubb Physica, 60 (Lx) (2015), pp. 13–24 2.

[3] Valentina Nicolini, Elisa Gambuzzi, Gianluca Malavasi, Ledi Menabue, Maria Cristina Menziani, Gigliola Lusvardi, Alfonso Pedone, Francesco Benedetti, Paola Luches, Sergio D'Addato, Sergio Valeri, Evidence of catalase mimetic activity in Ce^{3+}/Ce^{4+} doped bioactive glasses, J. Phys. Chem. B 119 (2015) 4009−−4019.

[4] Kenton P. Arkill, Richard E. Palmer, Jamie R. Lead, A high-resolution study of dynamic changes of Ce_2O_3 and CeO_2 nanoparticles in complex environmental media, Ruth C. Merrifield, Environ. Sci. Technol. 51 (14) (2017) 8010–8016.

[5] N.V. Skorodumova, S.I. Simak, B.I. Lundqvist, I.A. Abrikosov, B. Johansson, Quantum origin of the oxygen storage capability of ceria, Phys. Rev. Lett. 89 (16) (2002 Oct 14) 16660.

[6] Sameer Deshpande, Swanand Patil, Satyanarayana V.N.T. Kuchibhatla, Sudipta Seala, Size dependency variation in lattice parameter and valency states in nanocrystalline cerium oxide, Appl. Phys. Lett. 87 (2005) 133113.

[7] Maria Rita Cicconia, R. Daniel, Neuvilleb Wilfried, Blancc Jean-Francois, Lupic Manuel, Vermillacc Dominiquede Lignya, Cerium/aluminum correlation in aluminosilicate glasses and optical silica fiber preforms, J. Non-Cryst. Solids 475 (2017) 85–95.

[8] B. Bulfin, A.J. Lowe, K.A. Keogh, B.E. Murphy, O. Lübben, S.A. Krasnikov, I.V. Shvets, Analytical model of CeO_2 oxidation and reduction, J. Phys. Chem. C 117 (46) (2013) 24129–24137.

[9] Xin-Yuan Suna, Zhuo-Hao Xiaob, Yun-Tao Wuc, Zhitao Kangd, Fast Ce3+-activated borosilicate glass scintillators prepared in air atmosphere, Ceram. Int. 43 (2017) 3401–3404.

[10] Zhenlin Wang, Laifei Chenga, Structural evolution of CeO_2-doped alkali boroaluminosilicate glass and the correlation with physical properties based on a revised structural parameter analysis, RSC Adv. 6 (2016) 5456.

[11] G. Yang, S. Cook, R.J. Hand, G. Möbus, CeO_2 nano-precipitation in borosilicate glasses: a redox study using EELS, J. Eur. Ceram. Soc. 30 (4) (March 2010) 831–838.

[12] Katherine M. Dunnick, Rajalekshmi Pillai, Kelly L. Pisane, Aleksandr B. Stefaniak, Edward M. Sabolsky, Stephen S. Leonard, Biol trace, the effect of cerium oxide nanoparticle valence state on reactive oxygen species and toxicity, Elem. Res. 166 (1) (2015) 96–107 Published online 2015 Mar 17 https://doi.org/10.1007/s12011-015-0297-4.

[13] Soumen Das, Janet M Dowding, Kathryn E Klump, James F McGinnis, William Self 2 & Sudipta Seal, Cerium oxide nanoparticles: applications and prospects in nanomedicine, Nanomedicine 8, 9, 1483–1508.

[14] Zhang Rui, Hang Lin, Yu Yunlong, Xu Ju Chen Danqin, Wang Yuansheng, A new-generation color converter for high-power white LED: transparent Ce^{3+}:YAG phosphor-in-glass, Laser Photonics Rev. 8 (1) (2014) 158–164.

[15] G. Leonelli, G. Lusvardi, L. Malavasi, M. Tonelli Menabue, Synthesis and characterization of cerium-doped glasses and in vitro evaluation of bioactivity, J. Non-Cryst. Solids 316 (2–3) (February 2003) 198-216 C.

[16] A.J. Salinas, S. Shruti, G. Malavasi, L. Menabue, M. Vallet-Regí, Substitutions of cerium, gallium and zinc in ordered mesoporous bioactive glasses, Acta Biomater., 7, 9, 3452–3458.

[17] Milica PešićÅL, Ana Podolski-RenicÅL, Sonja StojkovicÅL, Branko MatovicÅL, Danica Zmejkoski, Å.L. Vesna Kojic, Å.L. Gordana Bogdanovic, Aleksandra Pavic ÅLevic ÅL, Å.L. Miloš Mojovic, Å.L. Aleksandar Savic, Å.L. Ivana Milenkovic, Aleksandar Kalauzi, Å.L. Ksenija Radotic, Anti-cancer effects of cerium oxide nanoparticles and its intracellular redox activity, Chem. Biol. Interact. 232 (2015) 85–93.

[18] Bryant C. Nelson, Monique E. Johnson, Marlon L. Walker, Kathryn R. Riley, Christopher M. Sims, Antioxidant cerium oxide nanoparticles in biology and medicine, Antioxidants 5 (2016) 15.

[19] Swetha Barkam, Julian Ortiz, Shashank Saraf, Nicholas Eliason, Rameech Mccormack, Soumen Das, Ankur Gupta, Craig Neal, Alex Petrovici, Cameron Hanson, Michael D. Sevilla, Amitava Adhikary, Sudipta Seal, Modulating the catalytic activity of cerium oxide nanoparticles with the anion of the precursor salt, J. Phys. Chem. C 121 (2017) 20039–20050.

[20] US Patent WO 2016 040480 A1, Delbert E.Day, Mohommad Kah Ali, March 2016.

[21] Emilie Janots, Emilie Janots, Felix Bernier, Fabrice Brunet, Manuel Muñoz, Nicolas Trcera, Alfons Berger, Martine Lanson, Ce(III) and Ce(IV) (re)distribution and fractionation in a laterite profile from Madagascar: insights from in situ XANES spectroscopy at the Ce L_{III}-edge, Geochim. Cosmochim. Acta 153 (2015) 134–148.

[22] Tian-Shuai Lv, Xu Xu-Hui, Yu Xue, Yu Hong-Ling, Da-Cheng Zhou Da-JianWang, Jian-Bei Qiu, Tunable full-color emitting borosilicate glasses via utilization of Ce3+ ions as multiple energy transfer contributors, J. Non-Cryst. Solids 385 (2014) 163–168.

[23] D.J. Smythe, J.M. Brenan, N.R. Bennett, T. Regier, G.S. Henderson, Quantitative determination of cerium oxidation states in alkali-aluminosilicate glasses using M4,5-edge XANES, J. Non-Cryst. Solids 378 (2013) 258–264.

[24] F. Zhang, P. Wang, J. Koberstein, S. Khalid, S.W. Chan, Cerium oxidation state in ceria nanoparticles studied with X-ray photoelectron spectroscopy and absorption near edge spectroscopy, Surf. Sci. 563 (2004) 74–82.

[25] Juarez L.F. Da Silva, Stability of the Ce_2O_3 phases: a DFT+U investigation, Phys. Rev. B 72 (2005) 205118.

[26] H. Shrnighaljsen, G. Schiller, The crystal structure of A-Ce_2O_3, Physica B 299 (2001) 180–186.

[27] Sergey M. Kozlov, Ilker Demiroglu, Konstantin M. Neyman, Stefan T. Bromley, Reduced ceria nanofilms from structure prediction, Nanoscale 7 (2015) 4361.

[28] David C. Grinter, Roslinda Ithnin, Chi L. Pang, Geoff Thornton, Defect structure of ultrathin ceria films on Pt(111): atomic views from scanning tunnelling microscopy, J. Phys. Chem. C 114 (2010) 17036–17041.

[29] Zhong Lin Wang, J. Xiangdong Feng, Polyhedral shapes of CeO_2 nanoparticles, Phys. Chem. B 107 (2003) 13563–13566.

[30] S. Tsunekawa, S. Ito, Y. Kawazoe, Surface structures of cerium oxide nanocrystalline particles from the size dependence of the lattice parameters, Appl. Phys. Lett. 85 (17) (25 October 2004) 0003-6951.

[31] R.K. Hailstone, A.G. DiFrancesco, J.G. Leong, T.D. Allston, K.J. Reed, A study of lattice expansion in CeO_2 nanoparticles by transmission electron microscopy, J. Phys. Chem. C 113 (34) (2009) 15155–15159.

[32] Feng Zhang, Siu-Wai Chan, Jonathan E. Spanier, Ebru Apak, Qiang Jin, Richard D. Robinson, Irving P. Herman, Cerium oxide nanoparticles: size-selective formation and structure analysis, Appl. Phys. Lett. 80 (2002) 127.

[33] G. El-Damrawi, K. El-Egili, Characterization of novel CeO_2-B_2O_3 glasses, structure and properties, Physica B 299 (2001) 180.

[34] E.F. Medvedev, Determination of sodium borosilicate bands in the IR spectrum of a multicomponent batch, Glas. Ceram. 64 (9–10) (2007) 300–304.

[35] G.P. Singh, P. Kaur, S. Kaur, D.P. Singh, Investigation of structural, physical and optical properties of CeO_2-Bi_2O_3-B_2O_3 glasses, Phys. B Condens. Matter 407 (21) (2012) 4168–4172.

[36] Michael C. Weinberg, Glass forming ability and stability in simple systems, J. Non-Cryst. Solids 167 (1994) 81–88.

[37] A.A. Cabral, A.A.D. Cardoso, E.D. Zanotto, Glass-forming ability versus stability of silicate glasses. I. Experimental test, J. Non-Cryst. Solids 320 (2003) 1–8.

[38] C. Gautam, A.K. Yadav, A.K. Singh, Review on infrared spectroscopy of borate glasses with effects of different additives, ISRN Ceram. 2012 (2012) (2012) 428497.